Journal of the European Ceramic Society 41 (2021) 3452–3458

Contents lists available at ScienceDirect

Journal of the European Ceramic Society

journal homepage: www.elsevier.com/locate/jeurceramsoc

Structure and chemical bond characteristics of two low-ε_r microwave dielectric ceramics $LiBO_2$ (B = Ga, In) with opposite τ_f

Junqi Chen [a,b], Weishuang Fang [a,b], Laiyuan Ao [a,b], Ying Tang [a,b,*], Jie Li [a,b], Laijun Liu [a,b], Liang Fang [a,b,*]

[a] Guangxi Key Laboratory of Optical and Electronic Materials and Devices, College of Material Science and Engineering, Guilin University of Technology, Guilin, 541004, China

[b] Key Laboratory of Nonferrous Materials and New Processing Technology, Ministry of Education, Guilin University of Technology, Guilin, 541004, China

ARTICLE INFO

Keywords:
Microwave dielectric materials
Chemical bond theory
Positive τf
LTCC technology

ABSTRACT

Two novel microwave dielectric materials $LiBO_2$ (B = Ga, In) were synthesized by a solid-state reaction method. The orthorhombic structured $LiGaO_2$ sintered at 1075 °C for 4 h exhibits a relative density of 96.1 ± 0.2 % and dielectric properties, namely, $\varepsilon_r \sim 5.82 \pm 0.01$ (16.7 ± 0.1 GHz), $Q \times f = 24{,}500 \pm 2000$ GHz, and $\tau_f \sim$ -74.3 ± 2 ppm/°C. Meanwhile, the tetragonal structured $LiInO_2$ sintered at 920 °C for 4 h exhibits a relative density of 85.3 ± 0.2 % and dielectric properties, namely, $\varepsilon_r \sim 9.6 \pm 0.01$ (15.2 ± 0.1 GHz), $Q \times f =$ 39,600 ± 2000 GHz, and $\tau_f \sim 9.8 \pm 2$ ppm/°C. The dielectric properties were investigated by chemical bond theory, and results indicate that the τ_f value is closely related to the bond ionicity. The good chemical compatibility of $LiInO_2$ ceramics with silver electrodes makes it a potential material for LTCC technology.

1. Introduction

Recently, with the rapid development of modern society, 5 G wireless communication technology has played an indispensable role in optimizing emerging technologies such as the Internet of Things, cloud computing, and artificial intelligence (AI). Furthermore, microwave dielectric ceramics as key materials have been widely used as substrates, antenna, dielectric resonators, filters, capacitors, base-station, and oscillators in wireless and satellite communications [1–3]. Generally, microwave dielectric materials must exhibit a suitable dielectric constant (ε_r), a high quality factor ($Q \times f$), and a near zero temperature coefficient of resonant frequency (τ_f) to shorten the signal delays (for low-ε_r), reduce the size of device (for high-ε_r), lower the energy dispersion and maintain the temperature stability in device circuits, respectively [4–6]. The difficult issue is that the ε_r of a dielectric material has a specific value, which cannot simultaneously reduce the size of the device and shorten the signal delay time. Then, low-temperature co-fired ceramic (LTCC) technology emerged to reduce the size of microwave devices by fabricating highly integrated.

In general, LTCC technology requires dielectric materials to have low sintering temperatures (below the melting point of silver, i.e., 961 °C) and good compatibility with Ag electrodes. The low ε_r dielectric ceramics system must contain one or more cations with a relative low ionic polarizability, such as Li^+ (1.20 Å^3), Mg^{2+} (1.32 Å^3), Zn^{2+} (2.04 Å^3), B^{3+} (0.05 Å^3), Al^{3+} (0.79 Å^3), Ga^{3+} (1.50 Å^3), Si^{4+} (0.87 Å^3), Ge^{4+} (1.63 Å^3), Sn^{4+} (2.83 Å^3), and P^{5+} (1.72 Å^3) [7]. Some low dielectric constant microwave dielectric ceramics are shown in Table 1 [8–21]. $LiAlO_2$ with a simpler wurtzite derived structure, in which all atoms are tetrahedrally coordinated, reportedly has an extremely low ε_r (4.4) [21]. However, the high sintering temperature (>1400 °C) impedes its further application in LTCC technology. Several studies have been conducted to solve this problem. Zuo et al. [21] reported that $LiAlO_2$ ceramics with 3.0 wt% Li_2O-B_2O_3-SiO_2-CaO-Al_2O_3 glass exhibit $\varepsilon_r \sim 4.48$, $Q \times f = 35$, 540 GHz, $\tau_f \sim$ -53 ppm/°C and a relative low sintering temperature of 900 °C. Lan et al. reported that the partial substitution of $[Zn_{0.5}Si_{0.5}]^{3+}$ for Al^{3+} could improve the microstructure, obtained optimum microwave dielectric properties ($\varepsilon_r = 6.12$, $Q \times f = 56{,}986$ GHz and $\tau_f =$ -122 ppm/°C) in $LiAl_{0.96}(Zn_{0.5}Si_{0.5})_{0.02}O_2$ sintered at 1300 °C, and added $CaTiO_3$ and H_3BO_3 to further lower the τ_f and the sintering temperature and satisfy the requirements of LTCC technology [20].

Considering that Al^{3+}, Ga^{3+}, and In^{3+} ions have the same valence state and nearly the same electronegativity, we explored the microwave

* Corresponding authors at: Guangxi Key Laboratory of Optical and Electronic Materials and Devices, College of Material Science and Engineering, Guilin University of Technology, Guilin, 541004, China.

E-mail addresses: tangyinggl001@aliyun.com (Y. Tang), fanglianggl001@aliyun.com (L. Fang).

https://doi.org/10.1016/j.jeurceramsoc.2021.01.024
Received 1 November 2020; Received in revised form 6 January 2021; Accepted 10 January 2021
Available online 21 January 2021

dielectric properties of $LiGaO_2$ and $LiInO_2$ ceramics. $LiGaO_2$ has the same simple wurtzite-derived structure as $LiAlO_2$ and a band gap within 5.3–5.6 eV [22]. However, $LiInO_2$ crystallizes in the tetragonal $LiFeO_2$-type structure with a band gap of 3.7 eV [23]. $LiGaO_2$ and $LiInO_2$ have received considerable attention due to their applications in catalysis, luminescence, and energy storage [22–25], but their microwave dielectric properties have yet to be reported. *Mazharul* et al. reported that $LiGaO_2$ and $LiInO_2$ ceramics could be sintered within the sintering temperature 700 °C–1000 °C [22,26], indicating that they might be potential materials for LTCC technology. In this work, the sintering behavior, crystal structure, microstructure, chemical bond characteristics, Raman spectra, dielectric spectroscopy, and microwave dielectric properties of $LiBO_2$ (B = Ga, In) ceramics were investigated.

2. Experimental procedures

Raw materials of high purity rare-earth Li_2CO_3 (> 99.95 %), Ga_2O_3 (> 99.99 %), and In_2O_3 (> 99.99 %) were used to prepare $LiBO_2$ (B = Ga, In) ceramics via the conventional solid-state reaction process. Raw materials Ga_2O_3 and In_2O_3 were first dried at 80 °C for 12 h before weighing because of they easily absorb the moisture in air. Then, all the starting materials were weighed stoichiometrically and ball-milled for 4 h with alcohol as the medium. The dried mixtures were first calcined at 900 °C and 750 °C for 4 h at a heating rate of 5 °C/min to obtain the $LiGaO_2$ and $LiInO_2$ phases, respectively. Subsequently, the dried powders with 5 wt% polyvinyl alcohol (PVA) were pressed into green disks with a diameter of 10 mm and a height of 6 mm under the pressure of 6 tons of press scale. Finally, all the samples were first heated to 550 °C for 2 h to remove the PVA and then within sintering temperatures 860 °C–940 °C and 1000 °C - 1100 °C for 4 h to obtain $LiInO_2$ and $LiGaO_2$ ceramics, respectively.

The crystal structure of $LiBO_2$ (B = Ga, In) ceramics was investigated using X-ray diffraction (XRD, X'Pert PRO, Holland) with $CuK_{\alpha 1}$ radiation. The structural refinement based on the fine XRD data was investigated by using the FullProf software [27]. Further in-depth information about the crystal structure of $LiBO_2$ (B = Ga, In) was obtained by performing transmission electron microscopy (TEM, JME-2100 F) and high-resolution transmission electron microscopy images (HRTEM) together with selected area electron diffraction (SAED) patterns. Before scanning electron microscopy (SEM) was used to observe the microstructure, the best sintered $LiGaO_2$ and $LiInO_2$ ceramics were polished to a mirror surface with 30, 9, 3, 1 and 0.5 μm diamond pastes and thermally etched at a sintering temperature of 50 °C below the sintering temperature. The density was obtained via the Archimedes' method. The Raman spectra were investigated using a Raman spectrometer with a 532 nm line. The temperature-dependent dielectric characteristics were measured by an Agilent 4294A precision impedance analyzer equipped with a temperature controller. The permittivity and the dielectric loss were measured in the TE_{011} mode using the Hakki and Coleman method [28] and the network analyzer (Model N5230 A, Agilent Co., Palo Alto, California) at the frequency range of 10 MHz to 40 GHz. The τ_f values were evaluated as follows:

$$\tau_f = \frac{f_2 - f_1}{f_1 (T_2 - T_1)} \quad (1)$$

Where f_1 and f_2 represent the operating frequencies at room temperature and 85 °C, respectively.

3. Results and Discussion

Fig. 1 shows the XRD patterns of $LiBO_2$(B = Ga, In) ceramics together with the standard data of $LiGaO_2$ (JCPDS#23−359), and $LiInO_2$ (JCPDS#43−1131). All the diffraction patterns show sharp peaks, indicating the formation of a highly crystalline phase. In the $LiBO_2$ (B = Ga, In) ceramics system, the $LiGaO_2$ ceramics crystallize into an orthorhombic structure phase. However, as the In^{3+} into the B site, the $LiInO_2$ ceramics form a tetragonal structure phase. To better understand the effect of the B-site cation on the crystal structure, Rietveld refinement was performed on the fine XRD data of $LiBO_2$ ceramics. As shown

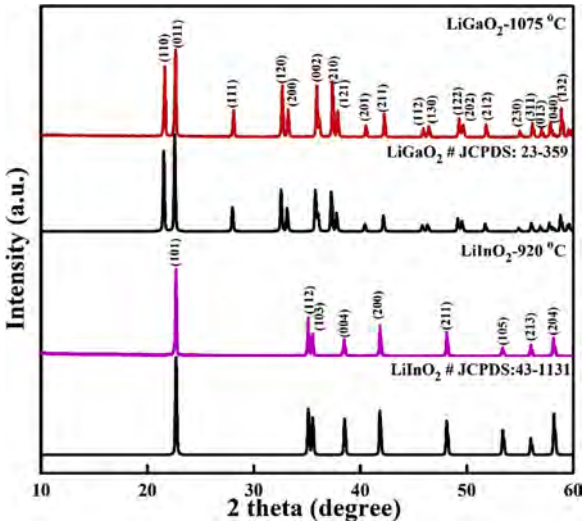

Fig. 1. XRD pattens of $LiBO_2$ (B = Ga, In) ceramics at their optimal sintering temperature.

Table 1
Some microwave dielectric ceramics with lower dielectric constant.

Compounds	*S.T.* (°C)	ε_r	$Q \times f$ (GHz)	τ_f (ppm/°C)	Reference
Li_2MgGeO_4	1220	6.1	28,500	−74.7	[8]
Li_2ZnGeO_4	1200	6.5	35,400	−60.6	[8]
$LiBGeO_4$	820	6.28	21,620	−88.7	[9]
$LiZnPO_4$	850	5.3	28,486	−80.4	[10]
$LiGa_5O_8$	1260	10.51	127,040	−60.16	[11]
Zn_2SiO_4	1250	6.7	27,917	−17	[12]
$Zn_2Ge_{1.1}O_4$	1060	7.09	112,700	−51	[13]
$Mg_{2.05}SiO_4$	1575	7.5	114,730	−59	[14]
$Mg_2Ge_{0.98}O_4$	1360	7.3	112,400	−64.6	[15]
Ca_2GeO_4	1420	6.76	82,400	−67	[16]
Ca_2SnO_4	1450	10.1	84,600	−42.5	[17]
$CaAl_2O_4$	1450	8.9	91,350	−55	[18]
$MgAl_2O_4$	1650	7.9	82,000	−73	[19]
$LiAl_{0.98}(Zn_{0.5}Ti_{0.5})_{0.02}O_2$	1300	6.45	56,986	−122	[20]
$LiAlO_2$ + 3 wt% LBSCA	900	4.48	35,540	−53	[21]
$LiGaO_2$	1075	5.82 ± 0.01	24,500 ± 2000	−74.3 ± 2	This work
$LiInO_2$	920	9.6 ± 0.01	39,600 ± 2000	9.8 ± 2	This work

in Figs. 2 (a) and (b), the good agreement between the observed and calculated XRD patterns coupled with low residual factors confirms that the refined lattice parameters and the unit cell volume summarized in Table 2 are acceptable. The crystal structures of $LiBO_2$(B = Ga, In) are shown in Figs. 2 (c) and (d). The Li and Ga atoms are located at the center of the oxygen tetrahedrons, forming an alternate stacking of two-dimensional arrays at the centers of the LiO_4 and GaO_4 tetrahedrons. However, in the tetragonal $LiInO_2$ system, Li, In, and O atoms occupy Wyckoff positions 4*b*, 4*a*, and 8*e*, respectively, in which each $(Li/In)O_6$ octahedron shares edges with six other $(Li/In)O_6$ octahedra. This phenomenon may be closely related to the radius of the trivalent cation. Generally, in the ABO_3 perovskite system, if the A-cation is smaller than what is required to form an ideal perovskite structure, the coordination of the A and B cations and the space group symmetry will be decreased and vice versa [29]. Therefore, as the large In^{3+}(CN = 6, 0.80 Å, CN = 4, 0.62 Å) enters the B-site, $LiInO_2$ forms a crystal structure with a higher coordination number and symmetry than those of $LiGaO_2$. TEM was used to further determine the crystal structure and phase composition of $LiBO_2$ (B = Ga, In) ceramic, as shown in Figs. S1 (a–d). The Raman spectra were used to investigate the lattice vibration modes, the phase composition, and the order-disorder, and the details are presented in the supplementary information and in Fig. S2.

The relationships between the density, relative density, and sintering temperature of the $LiBO_2$ (B = Ga, In) samples are shown in Fig. 3. Similar trends under increasing sintering temperature are shown in all compositions, that is, the density first increased from 3.85 ± 0.01 g/cm^{-3}, and 4.45 ± 0.01 g/cm^{-3} to a maximum 4.02 ± 0.01 g/cm^{-3}, 4.84 ± 0.01 g/cm^{-3}, respectively, and then gently decreased. At the optimum sintering temperature, the $LiBO_2$ (B = Ga, In) ceramics exhibited relative densities of 96.1 ± 0.2 % ($LiGaO_2$) and 85.3 ± 0.2 % ($LiInO_2$). SEM images of $LiGaO_2$ ceramics are shown in Figs. 4 (a–c). With the increase of sintering temperature, there is no obvious change of the grain shape. While, the average grain sizes of $LiGaO_2$ ceramics are increased from 2.7 μm to 3.8 μm. And a dense and homogeneous microstructure is exhibited at the optimum sintering temperature, which is consistent with the high relative density (96.1 ± 0.2 %). As shown in Figs. 4 (d–f), with the increase of sintering temperature, the average grain sizes of $LiInO_2$ ceramics are slightly increased from 2.1 μm to 2.6 μm. And all SEM images of $LiInO_2$ ceramics exhibit many pores at the grain boundary, which might be the main reason for its low relative density.

The phase purity and the crystal structure were investigated by XRD, TEM, and Raman spectroscopy. The results show that the B-site trivalent cation plays a dominant role in determining the crystal structure of $LiBO_2$ (B = Ga, In) ceramics. Therefore, their structure-properties relationship is worth exploring. The ε_r, $Q \times f$, and τ_f of $LiBO_2$ (B = Ga, In) ceramics as functions of sintering temperature are shown in Fig. 5. Both ε_r and $Q \times f$ values shown in Fig. 5 present a similar change tendency with the density. However, the τ_f value does not exhibit abrupt change with the sintering temperature.

To the best our knowledge, microwave dielectric properties are determined by the intrinsic lattice vibration and the extrinsic defects [30–32]. The former is contributed by the lattice anharmonic vibration and the latter are induced by the relative density, the secondary phases, the grain boundary, and the lattice defects. According to XRD and SEM analyses, the effect of the secondary phase could be ignored. To investigate the influence of porosity on ε_r, the following equation obtained by Penn et al. [33] is used to correct relative permittivity ε_r.

$$\varepsilon' = \varepsilon_m \left(1 - \frac{3P(\varepsilon_m - 1)}{2\varepsilon_m + 1}\right) \quad (2)$$

where ε_m is the permittivity of the material corrected for porosity, ε' is the experimentally obtained permittivity and P is the fractional porosity of $LiBO_2$ (B = Ga, In) ceramics, respectively. The corrected permittivity values, 6.1(6) and 11.7(6), were higher than the measured values, 5.82 ± 0.01, and 9.6 ± 0.01, at the optimum sintering temperature due

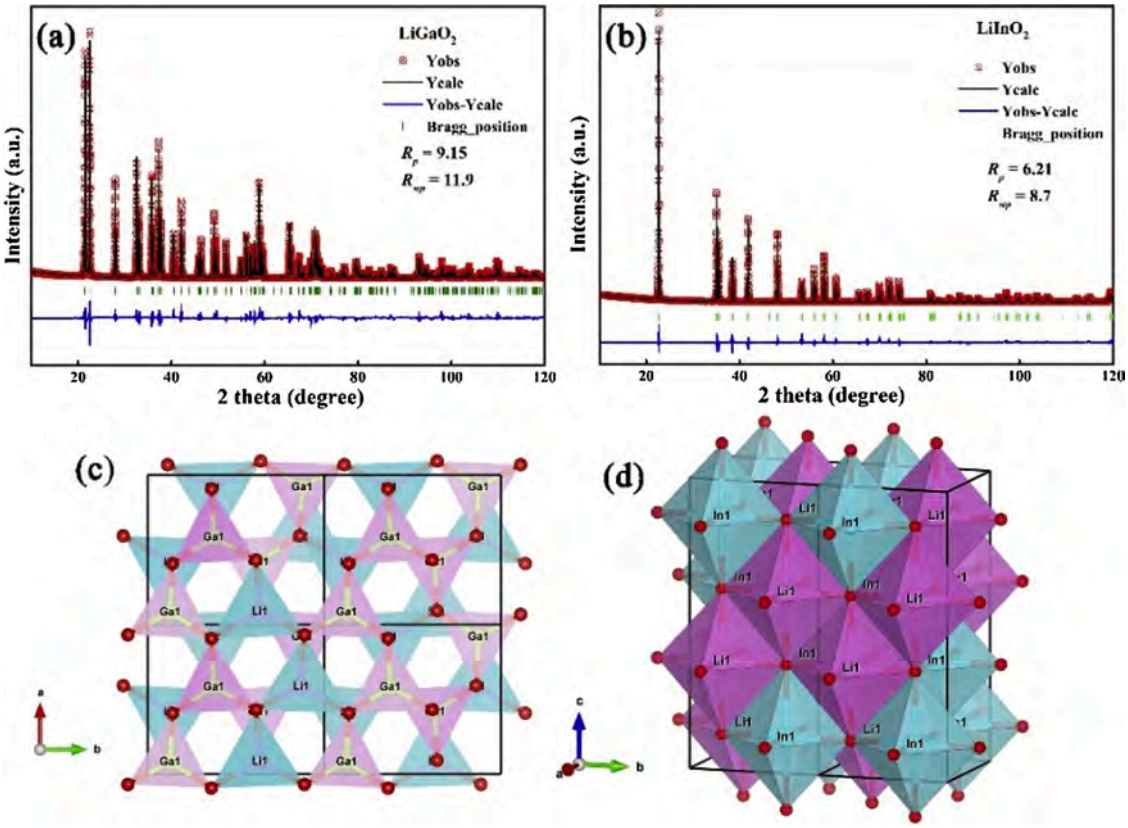

Fig. 2. Representative Rietveld refined X-ray diffraction data and crystalline structure for $LiBO_2$(B = Ga, In) ceramics.

Table 2
Space group, Rietveld refinement data, total ionic polarizability, theoretical, corrected, and experimental permittivity of $LiBO_2$(B = Ga, In) ceramics.

Compounds	Space group	a (Å)	b (Å)	c (Å)	v_m	α_D^T	$\varepsilon_{theoretical}$	$\varepsilon_{corrected}$	ε_r
$LiGaO_2$	Pna21	5.406(9)	6.379(1)	5.012(9)	172.89(7)	6.72	6.595(9)	6.1(6)	5.82 ± 0.01
$LiInO_2$	I41/amd	4.315(8)	4.315(8)	9.358(2)	174.30(4)	7.84	10.249(1)	11.7(6)	9.6 ± 0.01

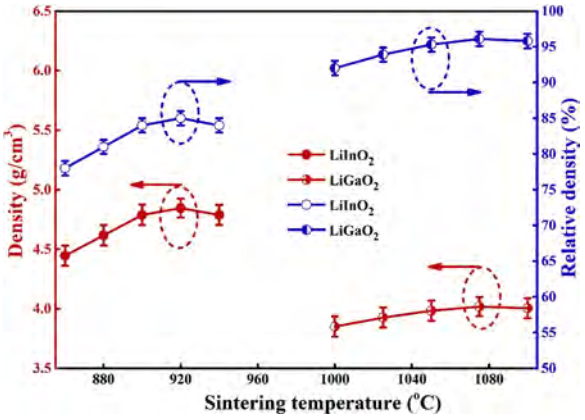

Fig. 3. Density and relative density of $LiBO_2$(B = Ga, In) samples as function of sintering temperature.

to the low dielectric of air. Furthermore, the Clausius-Mosotti [34] equation was used to calculated the intrinsic contribution caused by ionic polarizability. As shown in Table 3, the theoretical dielectric constant (ε_{th}, 6.595(9)) of the $LiGaO_2$ ceramic was higher than the corrected permittivity (i.e., 6.1(6)). This phenomenon can be explained by the crystal structure, in which LiO_4 and GaO_4 corner-shared formed a stable crystal structure, resulting in low ionic polarizability [35]. However, the corrected permittivity (ε_{th}, 11.7(6)) of $LiInO_2$ ceramic was higher than the theoretical dielectric constant (ε_{th}, 10.249(1)), which might be due to the rattling effects of the InO_6 and LiO_6 octahedron [36].

$LiInO_2$ has a larger $Q \times f$ value than $LiGaO_2$ and a near-zero τ_f value, which may be related to its crystal structure. To better understand the structure-properties relationships, the distortion (Δ), bond valence and packing fraction of $LiBO_2$ (B = Ga, In) ceramics were calculated and are summarized in Table 3. In previous research, a high packing fraction generally corresponds to a high $Q \times f$ values [37]. Therefore, the higher packing fraction of $LiInO_2$ (59.636(4)) than that of $LiGaO_2$ (53.905(5)) is the decisive factor affecting $Q \times f$. As for the τ_f, previous works have explained it by octahedral distortion and the bond valence [38,39]. Generally, a large Δ plays an important role in enhancing the ionic polarizability and further influences the τ_f value, while a large bond valence corresponds to a stable crystal structure, which reduces the dielectric loss caused by non-harmonic oscillator vibration [40,41]. In the $LiBO_2$ system, the coordination number of cations and the symmetry of the crystal structure will increase as a large In^{3+} enters the B-site, and with the increase of the coordination number, the bond length between the cation and the anion will increases, resulting in large ionic polarizability and low bond valence. The result is in good agreement with the bond valance as shown in Table 3.

In this work, the temperature-dependence of permittivity was also used to explore the temperature coefficient of resonant frequency (τ_f). The relationship among the τ_f, τ_ε and α_l can be expressed by the following equation:

$$\tau_f = -\alpha_l - \frac{1}{2}\tau_\varepsilon \quad (3)$$

For dielectric ceramics, α_l is usually +10 ppm/°C. Therefore, τ_ε plays a decisive role in τ_f. Fig. 6 shows the temperature dependence of the relative permittivity of $LiBO_2$ (B = Ga, In) ceramics at 1k Hz, 10k Hz, 100k Hz and 1 M Hz. Generally, if the sample is can easily absorb moisture, a Debye relaxation peak will appear at 0 °C–100 °C [42]. To solve this problem, we tested the temperature dependence of relative permittivity again under the vacuum state from -50 °C - 250 °C as shown in the inset of Fig. 6. Then, the τ_ε values of 20 °C–100 °C were obtained based on the temperature dependence of relative permittivity. The calculated τ_f value of -74.(5) ppm/°C for $LiGaO_2$ is consistent with measured value -74.3 ± 2 ppm/°C at the microwave regions. However, a large deviation exists between the calculated value (0.(8) ppm/°C) and the experimental value (9.6 ± 2 ppm/°C) for $LiInO_2$ ceramic.

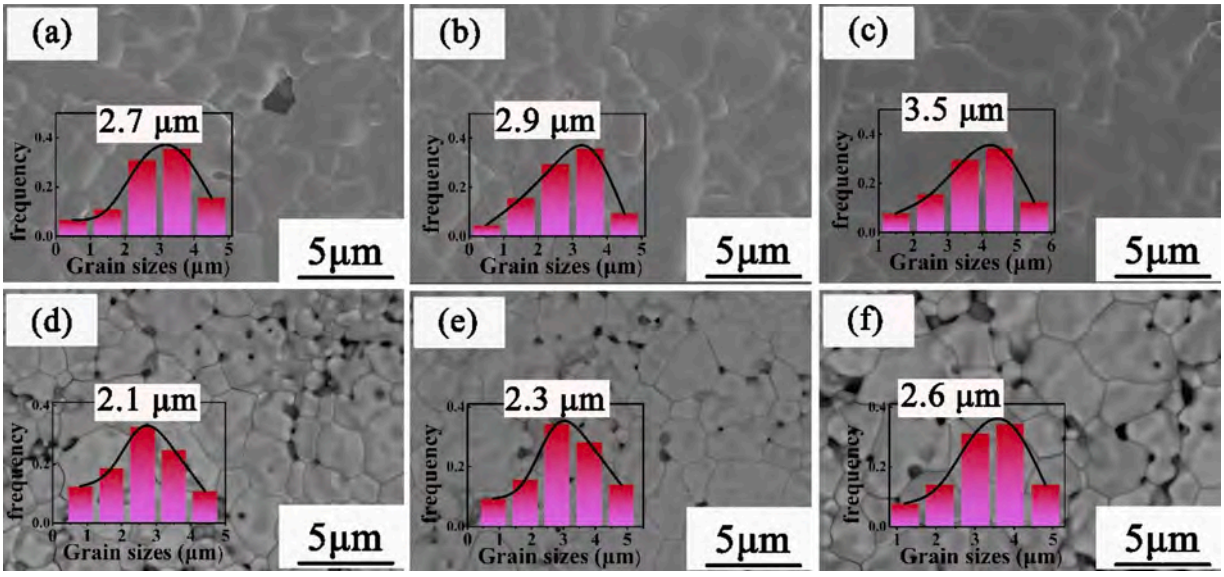

Fig. 4. SEM images of $LiBO_2$ (B = Ga, In) ceramics as function of sintering temperature: (a) $LiGaO_2$ - 1000 °C, (b) $LiGaO_2$ -1075 °C, (c) $LiGaO_2$ - 1100 °C, (d) $LiInO_2$ - 860 °C, (e) $LiInO_2$ - 920 °C, and (f) $LiInO_2$ - 940 °C. The statistic distributions of the gain size in ceramics using Gauss distribution.

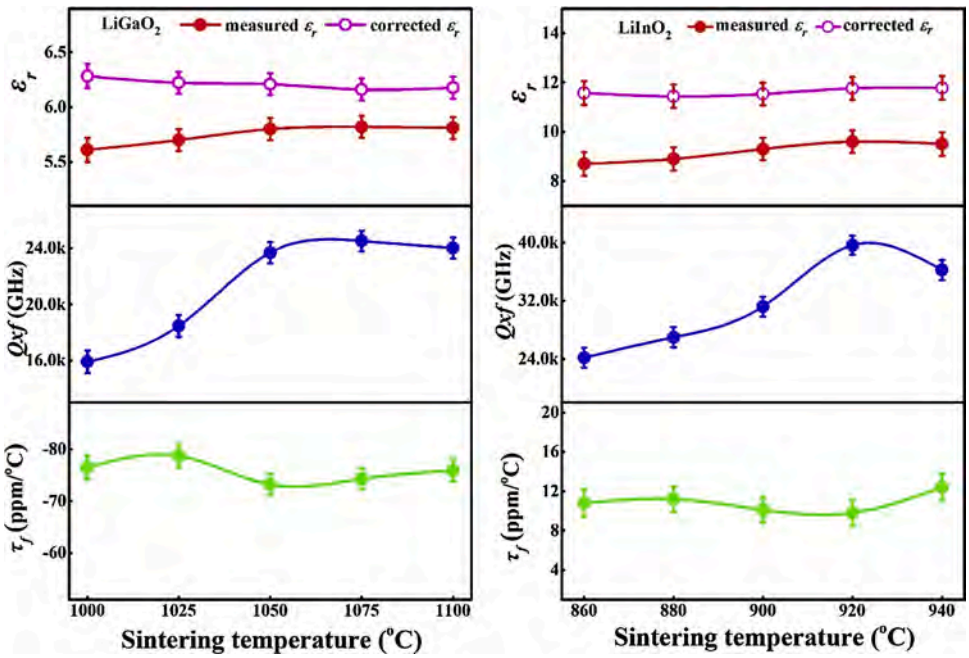

Fig. 5. Microwave dielectric properties ε_r, $Q\times f$, and τ_f of $LiBO_2$(B = Ga, In) samples as function of sintering temperature.

Table 3
Distortion degree (Δ), bond valence and packing fraction of $LiBO_2$(B = Ga, In) ceramics.

Compounds	Δ (Li)	Δ (B)	V_{Li} (Å)	V_B (Å)	V_{O1} (Å)	V_{O2} (Å)	Packing fraction (%)
$LiGaO_2$	$5.3(2)*10^{-4}$	$4.7(2)*10^{-6}$	0.990(3)	2.933(8)	1.920(6)	2.098(5)	53.905(5)
$LiInO_2$	$1.44(8)*10^{-3}$	$1.44(8)*10^{-3}$	0.806(9)	2.625(4)	1.714(1)	–	59.636(4)

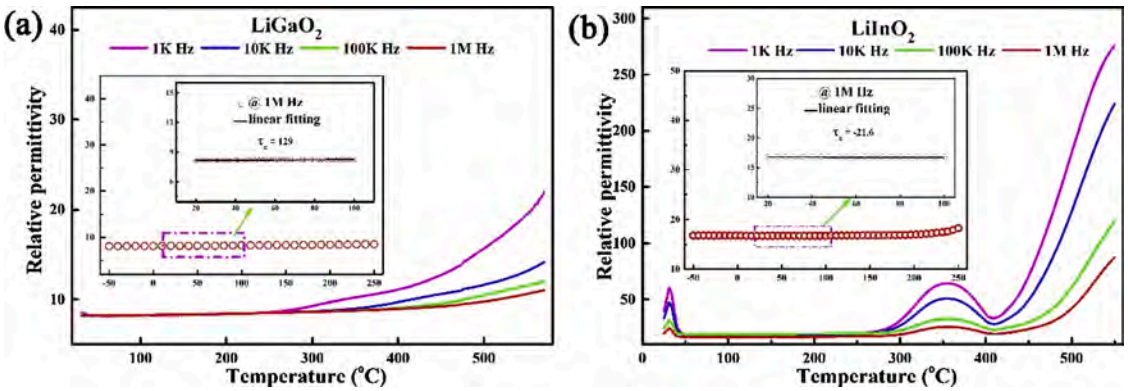

Fig. 6. Dependence of relative permittivity (ε_r) of $LiBO_2$(B = Ga, In) samples on temperature at 1 kHz, 10 kHz, 100 kHz, and 1 MHz, (a) $LiGaO_2$ sintered at 1075 °C and (b) $LiInO_2$ sintered at 920 °C.

To further understand the structure-properties relationships, the chemical bond characteristics of $LiBO_2$ (B = Ga, In) ceramics were investigated based on the (P—V—L) bond theory proposed by Phillips, Van Vechten, and Levine [43–46]. The bond length, chemical bond ionicity (f_i), lattice energy (U), and coefficient of thermal expansion α of $LiBO_2$(B = Ga, In) ceramics were obtained based on the PVL theory (Supplementary information) as shown in Fig. 7 and Table S1. Figs. 7(a) and (b) illustrate that the bond length and bond ionicity of $LiInO_2$ ceramics are higher than those of $LiGaO_2$, which are consistent with the ε_r of $LiInO_2$, which is much higher than that of $LiGaO_2$. Wu et al. [47,48] reported that the $Q \times f$ value has a strong connection with lattice energy (U). Usually, a high lattice energy corresponds to a strong bond, resulting in low dielectric loss. However, in the $LiBO_2$ system, the large In^{3+} enters the B-site increasing the coordination number of cations, improving the symmetry of crystal structure, and increasing the bond length, resulting in low lattice energy and high packing fraction. Fig. 7 (d) shows that the Li-O bonds of $LiGaO_2$ and $LiInO_2$ contribute the most to the coefficient of thermal expansion α.

To satisfy the requirements of LTCC technology, the chemical compatibility of $LiInO_2$ ceramics with silver electrodes was investigated. Fig. 8 shows the XRD pattern and BSE image analyses of $LiInO_2$ ceramics with 20 wt% Ag powders after co-firing at 900 °C for 2 h. As shown in Fig. 8(a), only the peaks of $LiInO_2$ and Ag were detected in the XRD patterns. The SEM micrograph exhibits some bright Ag grains distributed randomly among the $LiInO_2$ matrix, suggesting that the $LiInO_2$ ceramic did not react with the silver powders. Then, elemental mapping (Fig. S3) analysis further identified that the $LiInO_2$ ceramics are chemically compatible with silver electrodes and can be a potential material

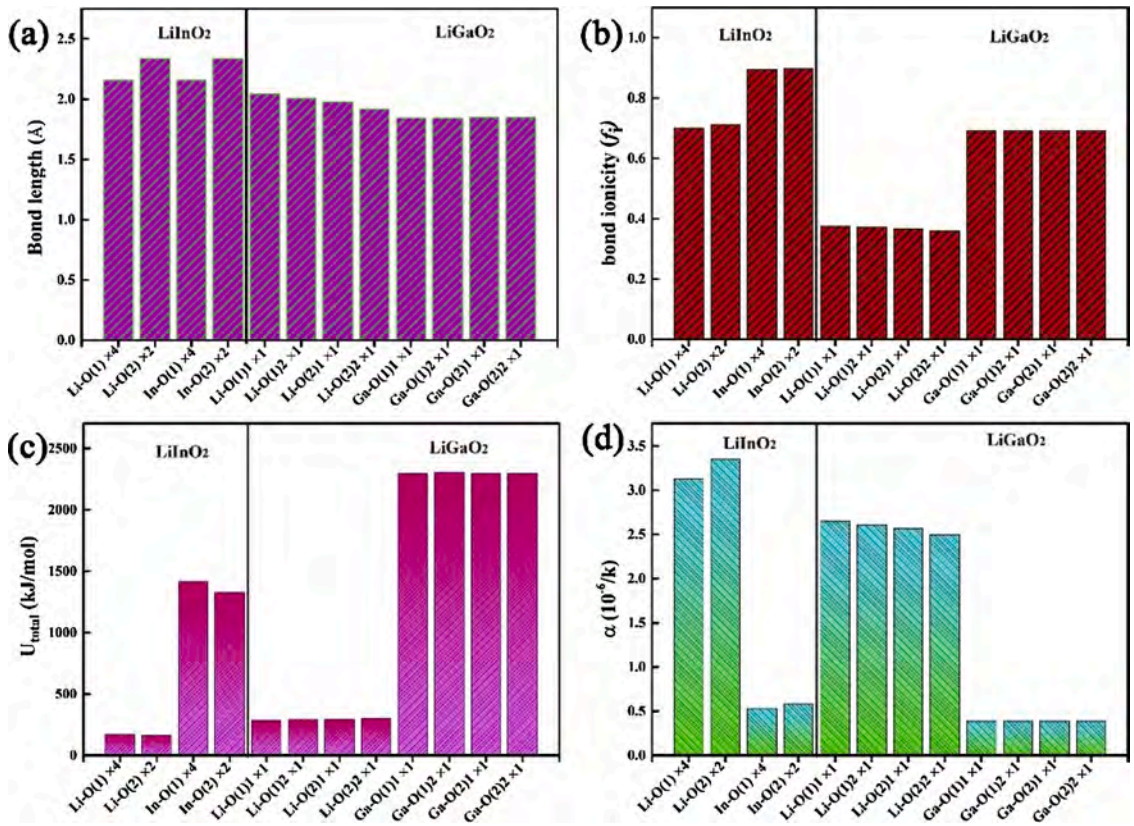

Fig. 7. Chemical bond parameters of $LiBO_2$(B = Ga, In) ceramics: (a) Bond length, (b) chemical bond ionicity (f_i), (c) lattice energy (U), and (d) coefficient of thermal expansion (α).

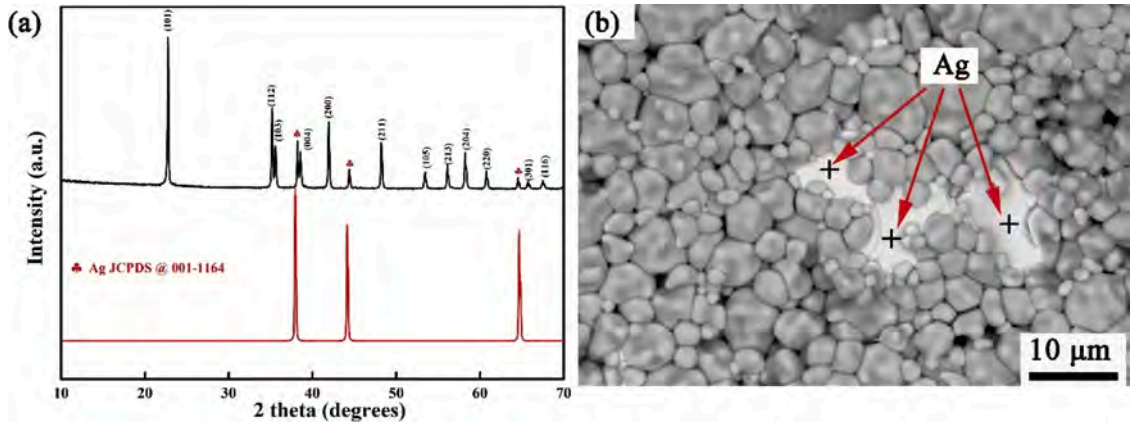

Fig. 8. (a) X-ray diffraction patterns, and (b) Backscattered electron image micrograph of $LiInO_2$ ceramic with 20 wt% silver powder.

for LTCC technology.

4. Conclusions

In this study, $LiBO_2$ (B = Ga, In) ceramics were prepared by the conventional solid-state route. XRD and TEM analyses indicate that the $LiGaO_2$ ceramics crystallized into the orthorhombic structure phase, and the $LiInO_2$ ceramics formed a tetragonal structure phase. In the $LiBO_2$ system, the large In^{3+} enters the B-site, increasing the coordination numbers of Li and B cations ($N_{CLi} = N_{CGa} = 4$ in $LiGaO_2$, and $N_{CLi} = N_{CIn} = 6$ in $LiInO_2$), improving the symmetry of the crystal structure, and increasing the bond length, resulting in low lattice energy and high packing fraction from 53.905(5)% of $LiGaO_2$ to 59.636(4)% of $LiInO_2$. The sintering temperature of $LiInO_2$ ceramics is lower than that of $LiGaO_2$ ceramics by 140 °C. The optimum microwave dielectric properties of $LiGaO_2$ were obtained at the sintering temperature of 1075 °C for 4 h, namely, $\varepsilon_r \sim 5.82 \pm 0.01$ (16.7 ± 0.1 GHz), $Q \times f = 24{,}500 \pm 2000$ GHz, and $\tau_f \sim$ -74.3 ± 2 ppm/°C. The $LiInO_2$ sintered at 1075 °C for 4 h exhibits microwave dielectric properties with $\varepsilon_r \sim 9.6 \pm 0.01$(15.2 ± 0.1 GHz), $Q \times f = 39{,}600 \pm 2000$ GHz, and $\tau_f \sim 9.8 \pm 2$ ppm/°C. The large bond ionicity and α value of the Li-O and In-O bonds might be the main reasons for the positive τ_f values of $LiInO_2$ ceramics. The $LiInO_2$ ceramics exhibit a good chemical compatibility with Ag electrodes and might therefore be a potential material for LTCC technology.

Declaration of Competing Interest

The authors declare that they have no known competing financial interests or personal relationships that could have appeared to influence the work reported in this paper.

Acknowledgments

The authors acknowledge the financial support from the Natural Science Foundation of China (Nos. 21965009 and 21761008) and Natural Science Foundation of Guangxi Zhuang Autonomous Region (Nos. 2018GXNSFAA138175 and 2018GXNSFAA281093). Project of Education Department of Guangxi Zhuang Autonomous Region (No. 2018KY0255), and Innovation Project of Guangxi Graduate Education (YCBZ2020066 and YCBZ2020167).

Appendix A. Supplementary data

Supplementary material related to this article can be found, in the online version, at doi:https://doi.org/10.1016/j.jeurceramsoc.2021.01.024.

References

[1] M.T. Sebastian, H.L. Jantunen, Low loss dielectric materials for LTCC applications: a review, Int. Mater. Rev. 53 (2008) 57–90.
[2] J.Q. Chen, Y. Tang, H.C. Xiang, L. Fang, H. Porwal, C.C. Li, Microwave dielectric properties and infrared reflectivity spectra analysis of two novel low-firing $AgCa_2B_2V_3O_{12}$ (B = Mg, Zn) ceramics with garnet structure, J. Eur. Ceram. Soc. 38 (2018) 4670–4676.
[3] D. Zhou, L.X. Pang, D.W. Wang, I.M. Reaney, $BiVO_4$ based high k microwave dielectric materials: a review, J. Mater. Chem. C Mater. Opt. Electron. Devices 6 (2018) 9290–9313.
[4] M.T. Sebastian, Dielectric Materials for Wireless Communication, Elsevier, 2015.
[5] H.C. Xiang, C.C. Li, Y. Tang, L. Fang, Two novel ultralow temperature firing microwave dielectric ceramics $LiMVO_6$(M=Mo, W) and their chemical compatibility with metal electrodes, J. Eur. Ceram. Soc. 37 (2017) 3959–3963.
[6] H.C. Xiang, C.C. Li, H. Jantunen, L. Fang, A.E. Hill, Ultralow loss $CaMgGeO_4$ microwave dielectric ceramic and its chemical compatibility with silver electrodes for low-temperature cofired ceramic applications, ACS Sustain. Chem. Eng. 6 (2018) 6458–6466.
[7] R.D. Shannon, Dielectric polarizabilities of ions in oxides and fluorides, J. Appl. Phys. 73 (1993) 348–366.
[8] C.C. Li, H.C. Xiang, M.Y. Xu, Y. Tang, L. Fang, Li_2AGeO_4 (A = Zn, Mg): two novel low-permittivity microwave dielectric ceramics with olivine structure, J. Eur. Ceram. Soc. 38 (2018) 1524–1528.
[9] Z. Xing, C.Z. Yin, Z.Z. Yu, J. Khaliq, C.C. Li, Synthesis of $LiBGeO_4$ using compositional design and its dielectric behaviors at RF and microwave frequencies, Ceram. Int. 46 (2020) 22460–22465.
[10] C.C. Xia, D.H. Jiang, G.H. Chen, Y. Luo, B. Li, C.L. Yuan, C.R. Zhou, Microwave dielectric ceramic of $LiZnPO_4$ for LTCC applications, J. Mater. Sci. Mater. Electron. 28 (2017) 12026–12031.
[11] L.Y. Ao, Y. Tang, J. Li, W.S. Fang, L. Duan, C.X. Su, Y.H. Sun, L.J. Liu, L. Fang, Structure characterization and microwave dielectric properties of $LiGa_5O_8$ ceramic with low-epsilon(r) and low loss, J. Eur. Ceram. Soc. 40 (2020) 5498–5503.
[12] N.H. Nguyen, J.B. Lim, S. Nahm, Effect of Zn/Si ratio on the microstructural and microwave dielectric properties of Zn_2SiO4 ceramics, J. Am. Ceram. Soc. 90 (2007) 3127–3130.
[13] C.Z. Yin, Y. Tang, J.Q. Chen, C.C. Li, L. Liang, F.H. Li, Y.J. Huang, Phase evolution, far-infrared spectra, and ultralow loss microwave dielectric ceramic of $Zn_2Ge_{1+x}O_{4+2x}$ ($-0.1 \le x \le 0.2$), J. Mater. Sci. Mater. Electron. 30 (2019) 16651–16658.
[14] K.X. Song, X.M. Chen, X.C. Fan, Effect of Mg/Si ratio on microwave dielectric characteristics of forsterite ceramics, J. Am. Ceram. Soc. 90 (2007) 1808–1811.
[15] J.Q. Chen, Y. Tang, C.Z. Yin, M.Y. Yu, H.C. Xiang, C.C. L, X.R. Xing, L. Fang, Structure, microwave dielectric performance, and infrared reflectivity spectrum of olivine type $Mg_2Ge_{0.98}O_4$ ceramic, J. Am. Ceram. Soc. 103 (2020) 1789–1797.
[16] Y. Tang, M.Y. Xu, L. Duan, J.Q. Chen, C.C. Li, H.C. Xiang, L. Fang, Structure, microwave dielectric properties, and infrared reflectivity spectrum of olivine type Ca_2GeO_4 ceramic, J. Eur. Ceram. Soc. 39 (2019) 2354–2359.
[17] K. Du, X.Q. Song, J. Li, W.Z. Lu, X.C. Wang, X.H. Wang, W. Lei, Phase compositions and microwave dielectric properties of Sn-deficient Ca_2SnO_4 ceramics, J. Alloys. Compd. 802 (2019) 488–492.
[18] B. Liu, C.C. Hu, Y.H. Huang, H.B. Bafrooei, K.X. Song, Crystal structure, infrared reflectivity spectra and microwave dielectric properties of $CaAl_2O_4$ ceramics with low permittivity, J. Alloys. Compd. 791 (2019) 1033–1037.
[19] C.Z. Zheng, S.Y. Wu, X.M. Chen, K.X. Song, Modification of $MgAl_2O_4$ microwave dielectric ceramics by Zn substitution, J. Am. Ceram. Soc. 90 (2007) 1483–1486.
[20] X.K. Lan, J. Li, Z.Y. Zou, G.F. Fan, W.Z. Lu, W. Lei, Lattice structure analysis and optimized microwave dielectric properties of $LiAl_{1-x}(Zn_{0.5}Si_{0.5})_xO_2$ solid solutions, J. Eur. Ceram. Soc. 39 (2019) 2360–2364.
[21] H.Z. Zuo, X.L. Tang, H.W. Zhang, Y.M. Lai, Y.L. Jing, H. Su, Low-dielectric-constant $LiAlO_2$ ceramics combined with LBSCA glass for LTCC applications, Ceram. Int. 43 (2017) 8951–8955.
[22] C.A. Lenyk, M.S. Holston, B.E. Kananen, L.E. Halliburton, N.C. Giles, Lithium and gallium vacancies in $LiGaO_2$ crystals, J. Appl. Phys. 124 (2018) 135702.
[23] A. Trukhin, L. Trinkler, Photoconductivity and photoelectron emission of $LiGaO_2$ crystal excited in intrinsic absorption range, Opt. Mater. (Amst) 93 (2019) 11–14.
[24] M.I. Mazharul, U. Johanna, W. Elena, S. Harald, H. Paul, B. Thomas, Lithium diffusion mechanisms in β-$LiMO_2$ (M = Al, Ga): a combined experimental and theoretical study, J. Phys. Chem. C 121 (2017) 27788–27796.
[25] Y. Liu, L.B. Tang, H.X. Wei, X.H. Zhang, Z.J. He, Y.J. Li, J.C. Zheng, Enhancement on structural stability of Ni-rich cathode materials by in-situ fabricating dual-modified layer for lithium-ion batteries, Nano Energy 65 (2019) 104043.
[26] S. Nanamatsu, K. Doi, M. Takhashi, Piezoelectric, elastic and dielectric properties of $LiGaO_2$, J. Appl. Phys. 6 (1972) 816–822.
[27] H.M. Rietveld, A profile refinement method for nuclear and magnetic structures, J. Appl. Crystallogr. 2 (1969) 65–71.
[28] B.W. Hakki, P.D. Coleman, A dielectric resonant method of measuring inductive capacitance in the millimeter range, IRE Trans Microwave Theory Technol. 8 (1960) 402–410.
[29] D.M. Giaquinta, H.C. Zurloye, Structural predictions in the ABO_3 phase piagram, Chem. Mater. 6 (1994) 6365–6372.
[30] S.H. Yoon, D.W. Kim, S.Y. Cho, K.S. Hong, Investigation of the relations between structure and microwave dielectric properties of divalent metal tungstate compounds, J. Eur. Ceram. Soc. 26 (2006) 2051–2054.
[31] D. Zhou, D. Guo, W.B. Li, L.X. Pang, X. Yao, D.W. Wang, I.M. Reaney, Novel temperature stable high-ε_r microwave dielectrics in the Bi_2O_3-TiO_2-V_2O_5 system, J. Mater. Chem. C Mater. Opt. Electron. Devices 4 (2016) 5357–5362.
[32] S. George, P.S. Anjana, V.N. Deepu, P. Mohanan, M.T. Sebastian, Low-temperature sintering and microwave dielectric properties of Li_2MgSiO_4 Ceramics, J. Am. Ceram. Soc. 92 (2009) 11244–11249.
[33] H.M. O'Bryan, J. Thomson Jr, J.K. Plourde, A new BaO-TiO_2 compound with temperature-stable high permitivity and low microwave loss, J. Am. Ceram. Soc. 57 (1974) 450–453.
[34] D. Hennings, P. Schnabel, Dielectric characterisation of $Ba_2Ti_9O_{20}$ type ceramics at microwave frequencies, Philips Res. J. 38 (1983) 295–311.
[35] J. Li, Y. Han, T. Qiu, C. Jin, Effect of bond valence on microwave dielectric properties of (1-x)$CaTiO_3$-$x(Li_{0.5}La_{0.5})TiO_3$ ceramics, Mater. Res. Bull. 47 (2012) 2375–2379.
[36] Y. Tang, Z.W. Zhang, J. Li, M.Y. Yu, Y.F. Zhai, L. Duan, C.X. Su, L.J. Liu, Y.H. Sun, L. Fang, $A_3Y_2Ge_3O_{12}$ (A = Ca, Mg): two novel microwave dielectric ceramics with contrasting τ_f and $Q \times f$, J. Eur. Ceram. Soc. 40 (2020) 3989–3995.
[37] E.S. Kim, B.S. Chun, R. Freer, R.J. Cernik, Effects of packing fraction and bond valence on microwave dielectric properties of ABO (A: Ca, Pb, Ba; B: Mo, W) ceramics, J. Eur. Ceram. Soc. 30 (2010) 1731–1736.
[38] N.E. Brese, M. OKeeffe, Bond-valence parameters for solids, Acta rystallogr. 47 (1991) 192–197.
[39] D. Zhou, J. Li, L.X. Pang, D.W. Wang, I.M. Reaney, Novel water insoluble $(Na_xAg_{2-x})MoO_4$ ($0 \le x \le 2$) microwave dielectric ceramics with spinel structure sintered at 410 degrees, J. Mater. Chem. C Mater. Opt. Electron. Devices 5 (2017) 6086–6091.
[40] H.T. Wu, Z.B. Feng, Q.J. Mei, J.D. Guo, J.X. Bi, Correlations of crystal structure, bond energy and microwave dielectric properties of $AZrNb_2O_8$ (A = Zn, Co, Mg, Mn) ceramics, J. Alloys. Compd. 648 (2015) 368–373.
[41] E.L. Colla, I.M. Reaney, N. Setter, Effect of structure changes in complex perovskites on the temperature coefficient of the relative permittivity, J. Appl. Phys. 74 (1993) 3414–3425.
[42] L.J. Liu, S.K. Ren, J. Zhang, B.L. Peng, L. Fang, D.W. Wang, Revisiting the temperature-dependent dielectric permittivity of $Ba(Ti_{1-x}Zr_x)O_3$, J. Am. Ceram. Soc. 101 (2018) 2408–2416.
[43] J.C. Phillips, J.A. Van Vechten, Charge redistribution and piezoelectric constants, Phys. Rev. Lett. 23 (1969) 1115–1117.
[44] J.C. Phillips, Ionicity of the chemical bond in crystals, Rev. Mod. Phys. 42 (1970) 317–356.
[45] B.F. Levine, A new contribution to the nonlinear optical susceptibility arising from unequal atomic radii, Phys. Rev. Lett. 25 (1970) 440–443.
[46] B.F. Levine, Bond susceptibilities and ionicities in complex crystal structures, J. Chem. Phys. 59 (1973) 1463–1486.
[47] H.T. Wu, E.S. Kim, Characterization of low loss microwave dielectric materials $Li_3Mg_2NbO_6$ based on the chemical bond theory, J. Alloys. Compd. 669 (2016) 134–140.
[48] Y.H. Zhang, H.T. Wu, Crystal structure and microwave dielectric properties of $La_2(Zr_{1-x}Ti_x)_3(MoO_4)_9$ ($0 \le x \le 0.1$) ceramics, J. Am. Ceram. Soc. 102 (2019) 4094–4102.